VOLUME I
AIRCRAFT PERFORMANCE

CHAPTER 10
HYPERSONIC AERODYNAMICS

APRIL 1987

USAF TEST PILOT SCHOOL
EDWARDS AFB CA

DISCLAIMER NOTICE

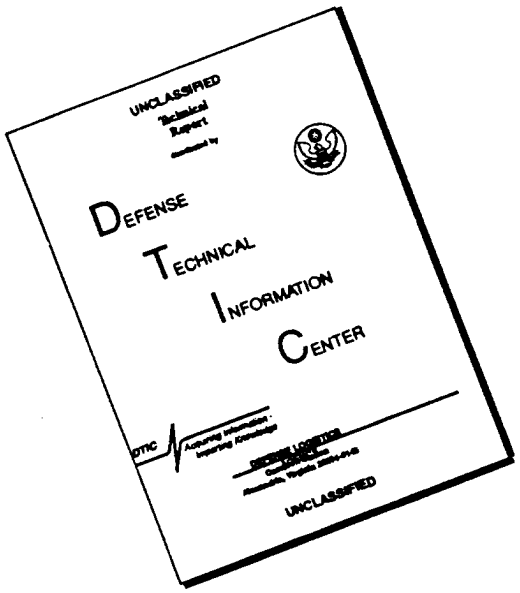

THIS DOCUMENT IS BEST QUALITY AVAILABLE. THE COPY FURNISHED TO DTIC CONTAINED A SIGNIFICANT NUMBER OF PAGES WHICH DO NOT REPRODUCE LEGIBLY.

14 HYPERSONIC AERODYNAMICS Page

14.1 INTRODUCTION

Earlier in supersonic aerodynamics, it was stated that a compressible, nonviscous, thermally perfect fluid was adequate for analysis of problems (outside of boundary layers) up to about Mach = 5.0. In this section we'll deal with problems above M = 5.0, especially as they relate to re-entry vehicles and hypersonic cruise vehicles.

As Mach changes from 4.99 to 5.01 nothing dramatic changes. Mach 5 is just a convenient rule of thumb. Hypersonic flow is best defined as the regime where certain physical flow phenomena become important. The actual Mach number where these physical phenomena become significant will vary with vehicle shape, Reynolds number, etc. These phenomena are:

a. Thin, curved shock layers (i.e. the region between the shock and body).
b. Strong viscous effects throughout the shock layer.
c. Low density effects resulting in a non-zero velocity at the surface (velocity slip).
d. High energy causing the fluid to behave in a non-thermally perfect manner.

When these phenomena become important, they significantly complicate the flow analysis problem. In addition to the normal problem of determining the pressure pattern around a vehicle in order to get lift, drag and stability derivatives, a new problem becomes important at hypersonic speeds: predicting the heat input into the vehicle caused by the high energy in the flow. This aspect is not a major concern at low Mach numbers but can be the dominant concern at hypersonic speeds (shooting stars make this obvious).

Therefore, this course is broken into two broad catagories: the aerodynamics of high Mach number flows (pressure pattern, lift, drag) and aerothermodynamics (temperature predictions, heat transfer). Further, the aerodynamics of high Mach flows will be subdivided into two sections for clarity. First, viscosity will be ignored to look at purely Mach number effects and then the viscous terms will be included to show their effects at low Reynolds numbers.

14.2 MACH NUMBER EFFECTS

As we saw in supersonic aerodynamics, the Mach number has a strong influence on shock waves and the fluid parameter changes across the shock. A hypersonic vehicle designed to achieve orbital velocities will transit a region including Mach numbers up to at least M = 25 (orbital velocity) and the very existence of these large Mach numbers can have a dominant effect on the flow. In this section the purely fluid dynamic effects of Mach number are discussed without the added complications of viscosity or other real gas effects.

14.2.1 Basic Hypersonic Shock Relations

If we ignore viscosity and assume a thermally perfect gas we have the same relations for fluid parameter changes across a shock that we developed in Chapter 6, Supersonic Aerodynamics. However for large Mach numbers, certain simplifying assumptions become possible.

For example, equation 6.49 from supersonic aerodynamics gives the relationship between density behind an oblique shock and the upstream density:

$$\frac{\rho_2}{\rho_1} = \frac{(\gamma + 1)\ M_1^2 \sin^2\theta}{2 + (\gamma - 1)\ M_1^2 \sin^2\theta}$$

If $M >> 1$ then M^2 dominates so the 2 in the denominator can be ignored and then the $M_1^2 \sin^2\theta$ terms cancel each other leaving:

$$\frac{\rho_2}{\rho_1} \approx \frac{\gamma + 1}{\gamma - 1} \qquad (14.1)$$

In similar fashion, the other basic relations across an oblique hypersonic shock wave reduce to

$$\frac{T_2}{T_1} \approx \frac{2\gamma\ (\gamma - 1)}{(\gamma + 1)^2}\ M_1^2 \sin^2\theta \qquad (14.2)$$

and

$$\frac{p_2}{p_1} \approx \frac{2\gamma}{\gamma + 1} M_1^2 \sin^2\theta \qquad (14.3)$$

Using the relationship between p_2 and p_1 can also give us a very simple result for the coefficient of pressure, C_p. Since C_p is defined as

$$C_p = \frac{p_2 - p_1}{q_1} = \frac{2}{\gamma M_1^2} \frac{P_2}{P_1} - 1$$

including the hypersonic approximation for p_2/p_1 gives:

$$C_p \approx \frac{4}{\gamma + 1} \sin^2\theta - \frac{2}{\gamma M_1^2}$$

or with $M_1 >> 1$,

$$C_p \approx \frac{4}{\gamma + 1} \sin^2\theta \qquad (14.4)$$

In addition, the relationship between the wave angle θ and the wedge angle δ is simplified. From Chapter 6 we had (equation 6.55),

$$\tan \delta = 2 \cot \theta \frac{M_1^2 \sin^2\theta - 1}{M_1^2(\gamma + \cos 2\theta) + 2}$$

This relationship was plotted in Figure 6.14. For small wedge angles the change in wave angle gets smaller and smaller as Mach increases. Figure 14.1 is an illustration. Using small angle approximations:

$$\sin \theta \approx \theta$$

$$\cos 2\theta \approx 1$$

$$\tan \delta \approx \delta$$

$$\cot \theta = \frac{1}{\tan \theta} \approx \frac{1}{\theta}$$

gives

$$\delta \approx \frac{2}{\theta} \frac{M_1^2 \theta^2 - 1}{M_1^2 (\gamma + 1) + 2}$$

if $M_1 >> 1$ then further

$$\delta = \frac{2}{\theta} \frac{M_1^2 \theta^2}{M_1^2(\gamma + 1)}$$

or

$$\delta = \frac{2\theta}{\gamma + 1} \qquad (14.5)$$

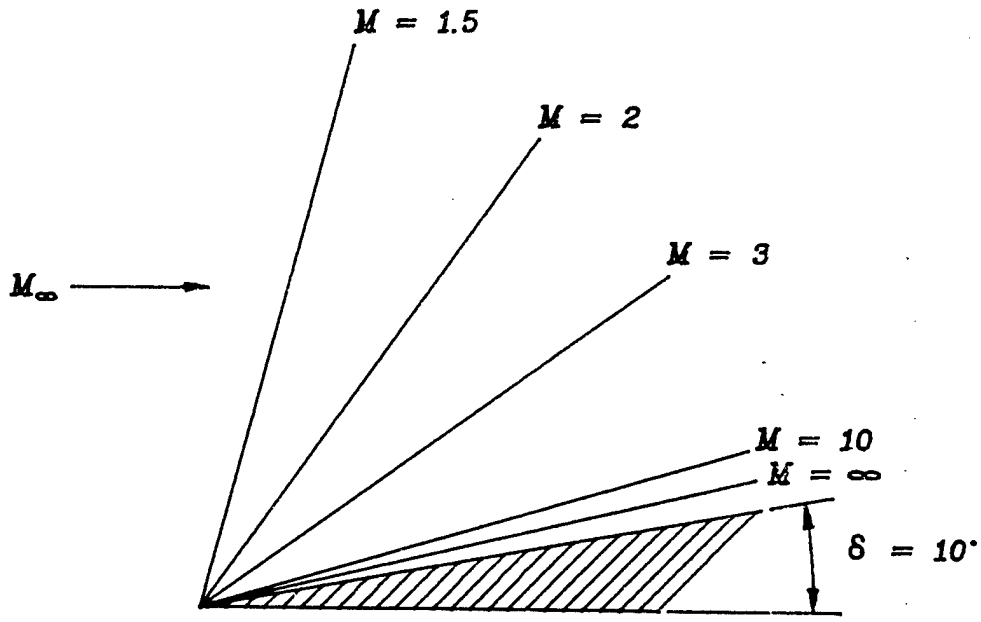

Figure 14.1 Shock Wave Angle at High Mach

Qualitatively speaking, then, the solution of hypersonic shock problems, ignoring viscous and other effects, is much simpler than for supersonic flow problems. As we'll see in the next sections, some calculations become extremely simple and fortunately give reasonable results for a limited category of real problems.

14.2.2 Mach Number Independence

As we just saw in the preceding section, some relationships become independent of Mach at hypersonic speeds. Examples are the density ratio across an oblique shock (equation 14.1) and the coefficient of pressure for a small wedge angle (equation 14.4).

Other relationships continue to depend on Mach number. From equation 14.2 and 14.3 it can be seen that the increase in pressure and temperature across an oblique shock both tend to ∞ as $M \to \infty$. If, however, we non-dimensionalize pressure with dynamic freestream pressure,

$$\overline{P}_2 = \frac{P_2}{\rho_1 V_1^2} = \frac{P_2}{P_1} \frac{1}{\gamma M_1^2}$$

then equation 14.3 can be rewritten as

$$\overline{P}_2 = \frac{1}{\gamma M_1^2} \frac{2\gamma}{\gamma + 1} M_1^2 \sin^2\theta$$

or

$$\overline{P}_2 = \frac{2}{\gamma+1} \sin^2\theta \qquad (14.6)$$

which is also independent of Mach.

In general, non-dimensional variables become independent of Mach at hypersonic speeds. Examples of this can be seen in figures 14.2, 14.3, and 14.4. In each of these examples the non-dimensional parametmeter C_D, L/D_{max}, or C_{n_β}) all vary dramatically transonically and supersonically, but once hypersonic speed is attained, the parameters no longer change with increasing Mach.

The obvious utility of this is emphasized in the last example, figure 14.4. Prior to the first launch of the space shuttle no wind tunnel data was available above M = 16 and very little above M = 8. While all parameters do not conform to the predictions as well as this example, most were similar.

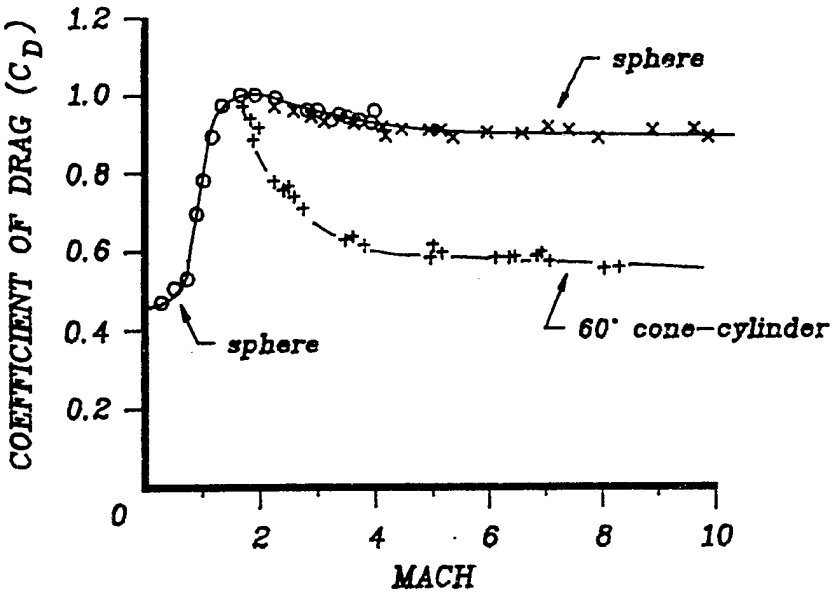

Figure 14.2 Experimental Drag Measurements (o Charters and Thomas (1945), × Hodges (1957), + Stevens (1950))

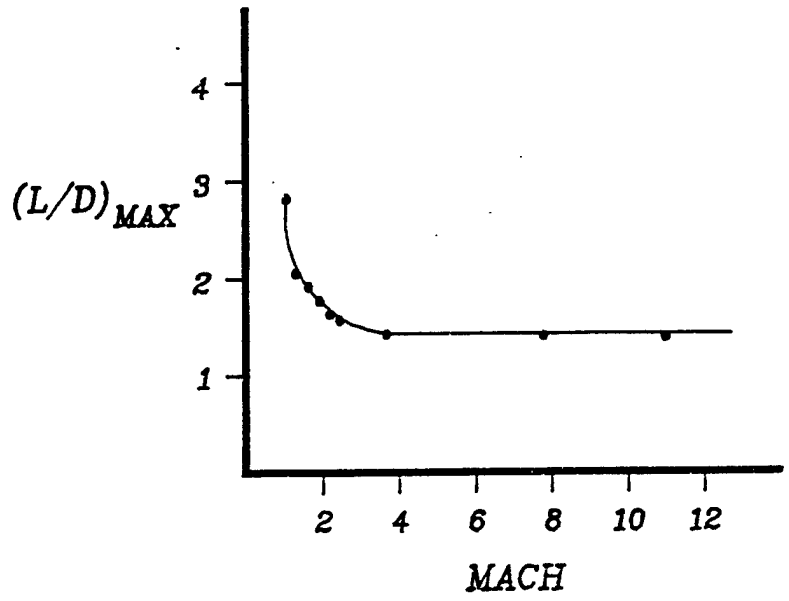

Figure 14.3 Wind–Tunnel Results for $(L/D)_{MAX}$ for an Integral Re–entry Body (Krogemann, 1973)

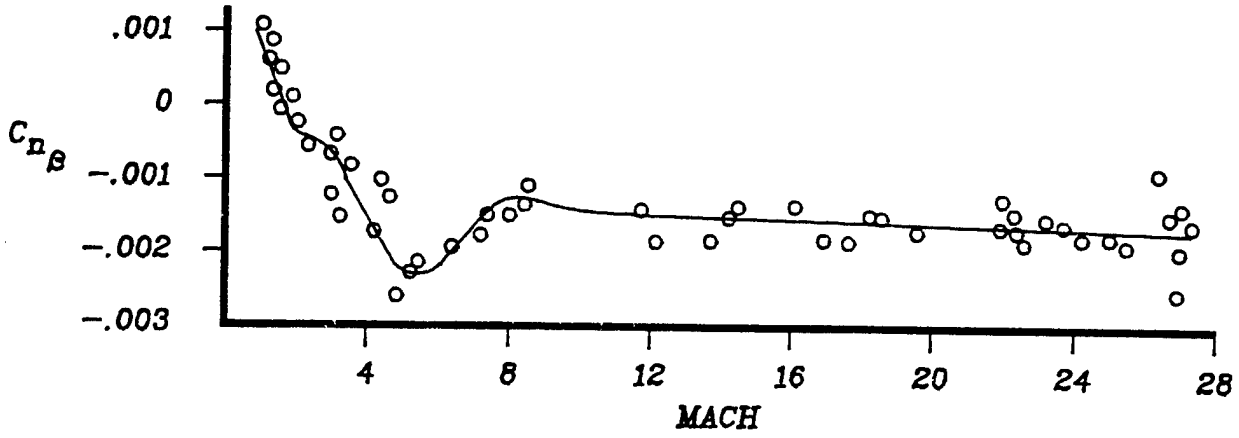

Figure 14.4 Space Shuttle Data for Yawing Moment due to Sideslip

14.2.3 Hypersonic Similarity

Similarity in aerodynamics refers to identifying parameters or combinations of parameters that result in identical fluid flow changes at different conditions. The advantage is obvious: you can do experimental tests at one set of conditions and then predict the results at another set of conditions. The criteria for hypersonic similarity can be derived mathematically (see references 2 or 3), but the following discussion should suffice to justify the use of similarity.

Consider a slender body in a hypersonic flow at a low angle of attack. These limitations allow use of small perturbation assumptions.

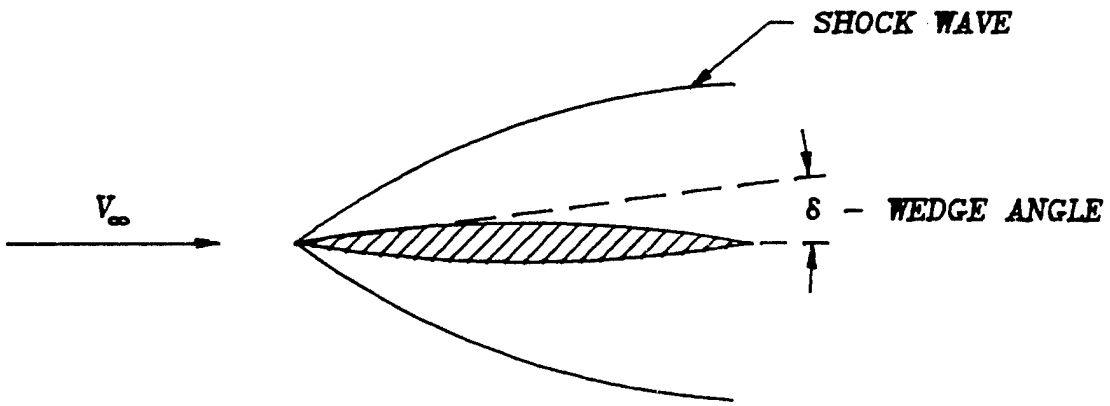

Figure 14.5 Slender Body in Hypersonic Flow

If we define the changes in velocity in the x and y directions as u' and v', then at some point downstream of the shock,

$$u = V_\infty + u'$$

$$v = v'$$

Over a slender body the change in the x component of the velocity is very small compared to the change in the y direction (0 to v' is a large percentage increase). Thus it can be seen as essentially a small deflection of the fluid either up or down. With this picture,

$$\sin \frac{v'}{V_\infty + u'} = \sin \delta$$

But since u' is assumed small in comparison to V_∞, then

$$\sin \frac{v'}{V_\infty} \simeq \sin \delta$$

or, if $v' << V_\infty$

$$\frac{v'}{V_\infty} \simeq \sin\delta$$

or

$$\frac{v'}{a_\infty} \simeq M_\infty \sin\delta .$$

Thus, a measure of the disturbance referenced to the freestream speed of sound is $M \sin\delta$. If two different flow problems have the same disturbance then they are similar and have like solutions. We can define this disturbance indicator as the hypersonic similarity parameter, K.

$$K \equiv M_\infty \sin\delta \tag{14.7}$$

In some texts K is defined as $M_\infty \tau$ where τ is the thickness ratio, d/ℓ. The thickness ratio for slender bodies is of the same order of magnitude as $\sin\delta$ and is equally good for stipulating hypersonic similarity.

Figure 14.6 and 14.7 are examples of data at different conditions that have the same hypersonic similarity parameter. These examples show the usefulness of hypersonic similarity within the small angle limitations.

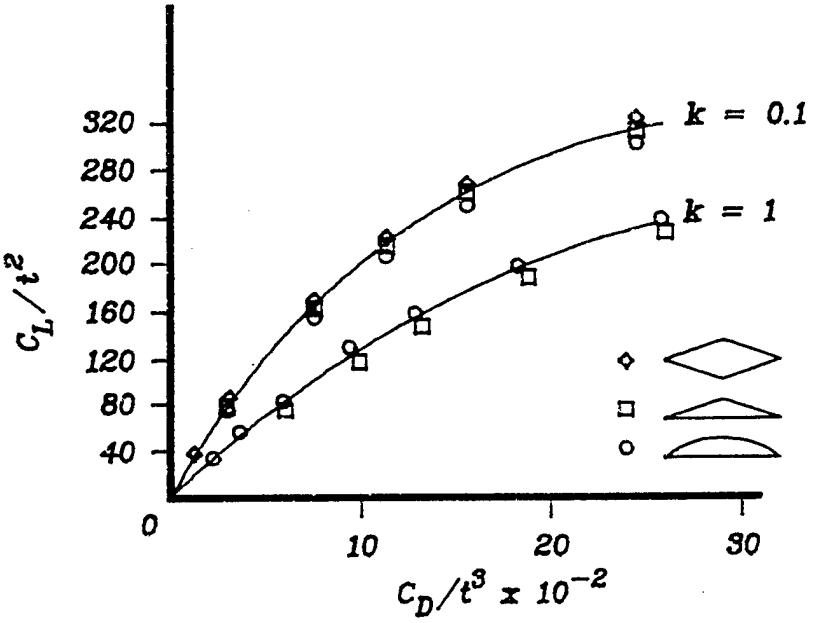

Figure 14.6 Analytically Derived Drag Polar Showing Hypersonic Similarity (Ref 2: pg 50)

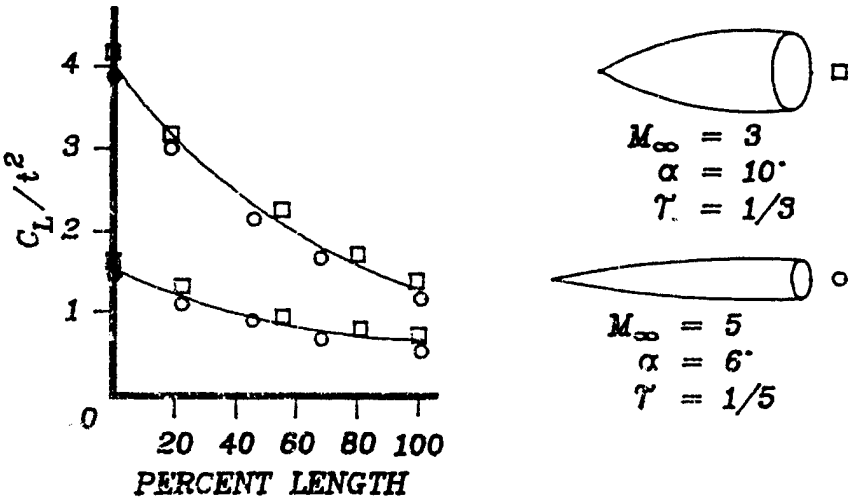

Figure 14.7 Pressure Ratios for Different Body Shapes with Hypersonic Similarity

14.2.4 Newtonian Theory

In 1687, Isaac Newton modeled fluid flow as a stream of particles that do not interact with each other. This concept is essentially a totally inviscid flow description, which gave very poor results when Newton tried to predict 17th century ship hull drag. His model, however, gives surprisingly good results when applied to some hypersonic problems. Isaac was just slightly ahead of his time.

The basic assumption that Newton used was that as each streamline of particles approached a body the streamline would be deflected to parallel the surface. Essentially this means that there will be a complete loss of normal momentum and no change in the tangential component of the momentum. Figure 14.8 shows this for a flat plate at some angle of attack. Here $V_{2_t} = V_{1_t} = V_2$ and $V_{2_n} = 0$.

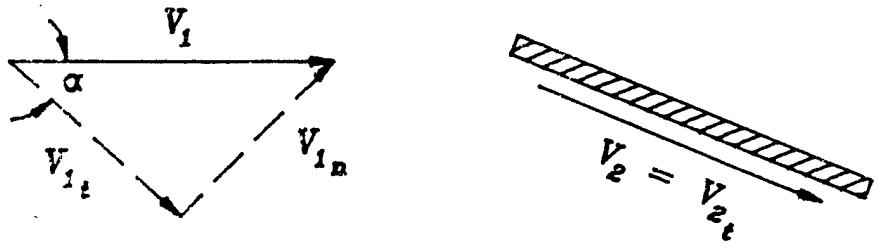

Figure 14.8 Newtonian Flow Over a Flat Plate

From Newton's second law, the time rate of change of momentum is equal to the force

$$\vec{F} = m \frac{\Delta \vec{V}}{\Delta t}$$

The only change in V is the total loss of the normal component of the momentum. Thus the force is normal to the surface with magnitude :

$$F = m \frac{(V_{n1} - 0)}{\Delta t}$$

For the flat plate in figure 14.8, this can be rewritten as

$$F = \frac{m}{\Delta t} V_1 \sin\alpha$$

The mass flow rate incident on a flat plate of area A is

$$\dot{m} = \rho_1 V A \sin\alpha$$

Therefore

$$F = (\rho_1 V_1 A \sin\alpha) V_1 \sin\alpha$$

Realizing that F/A is just $p_2 - p_1$, we can rewrite this as

$$F/A = p_2 - p_1 = \rho V_1^2 \sin^2\alpha$$

Finally, since the coefficient of pressure C_p, is just the static pressure change divided by the dynamic pressure, we get to Newton's result:

$$C_p = 2 \sin^2\alpha \qquad (14.6)$$

From this simple result we can quickly derive relationships for C_L, C_D, and L/D:

$$C_L = C_p \cos\alpha = 2 \sin^2\alpha \cos\alpha$$

$$C_D = C_p \sin = 2 \sin^3\alpha$$

and

$$L/D = C_L/C_D = \frac{1}{\tan\alpha}$$

While all of these answers gave poor results for 17th century sailing ships, figures 14.9 and 14.10 show good results when applied to some hypersonic problems.

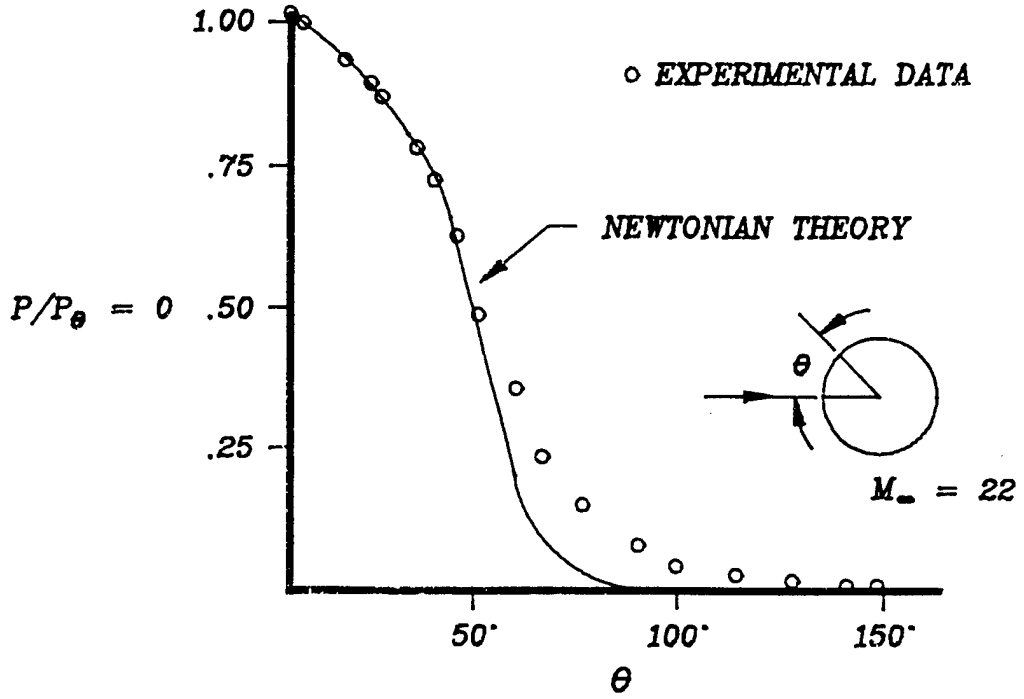

Figure 14.9. Pressure Distribution on a Circular Cylinder

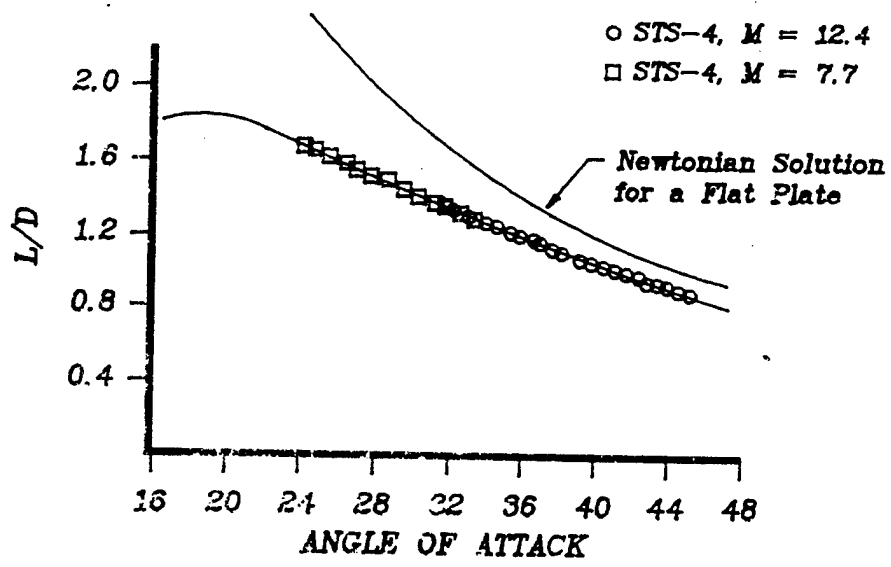

Figure 14.10 Lift–to–Drag Ratio for the Space Shuttle

Notice that the non-dimensional L/D ratio, C_L, and C_D do not change with Mach, in concert with the previous discussion of Mach number independence.

Newtonian theory's true physical significance can be seen by examining the exact oblique shock relationship for C_p in the following form (see Ref 4, page 10):

$$C_p = \frac{4}{\gamma + 1} \sin^2\theta - \frac{1}{M_1^2} \tag{14.9}$$

This exact (albeit inviscid) equation reduces to Newton's equation (14.8) when $\gamma \to 1$ and $M_1 \to \infty$.

14.3 VISCOUS EFFECTS

Viscous effects are ignored whenever possible. Including viscous terms greatly complicates the mathematical description of aerodynamic phenomena. In supersonic aerodynamics we ignored viscosity altogether, relegating it to a thin boundary larger which had a relatively minor contribution to changes in lift and drag at supersonic Mach numbers. The major idea that you should get from this section is that viscous effects cannot be so casually dealt with at hypersonic speeds.

14.3.1 The Boundary Layer

The boundary layer is a mathematical simplification. Outside of some distance to the body in a fluid flow we choose to ignore viscosity because it simplifies the flow problem without causing serious errors in our results: viscous effects are negligible. Inside the boundary layer, however, viscous effects must be included or our results will be significantly in error. Figure 14.11 in an illustration.

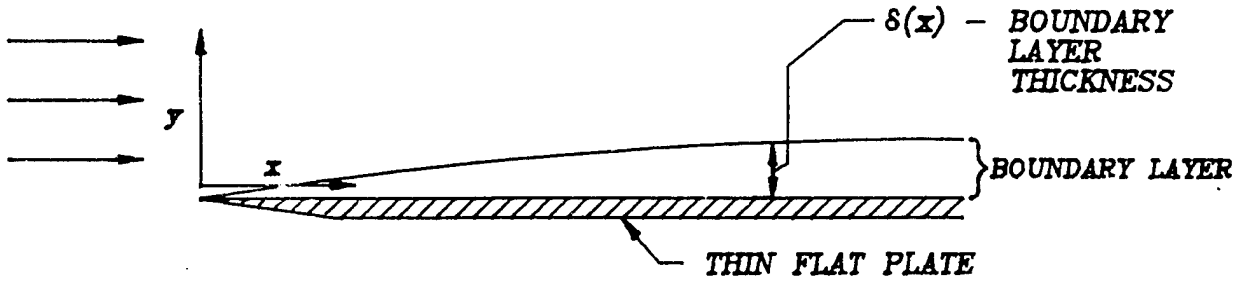

Figure 14.11 Boundary Layer

The main assumption that we made in supersonic aerodynamics was that the boundary layer thickness, δ, was small compared to the scale of the body. Hence ignoring it caused no serious errors. However, the thickness of the boundary layer varies not only with distance as shown in figure 14.11 but also with Mach and Reynolds numbers as :

$$\frac{\delta}{x} \propto \frac{M_\infty^2}{R_e} \qquad (14.10)$$

Thus the combinations of lower Reynolds numbers (high altitude flight) and, especially, high Mach (thickness grows as the square of M_∞) can produce hypersonic boundary layers orders of magnitude thicker than boundary layers at lower speeds.

There are, broadly speaking, two ways of dealing with this increased importance of viscosity: use boundary layer concepts or analytically treat the entire flow as viscous. These are the subjects of the next two brief sections.

14.3.2 Viscous Interaction

The thick boundary layers at hypersonic speeds lead to a major interaction between the growth of the boundary layer and the outer inviscid flow. A major consequence of this interaction is the effect on the pressure distribution, as shown in figure 14.12.

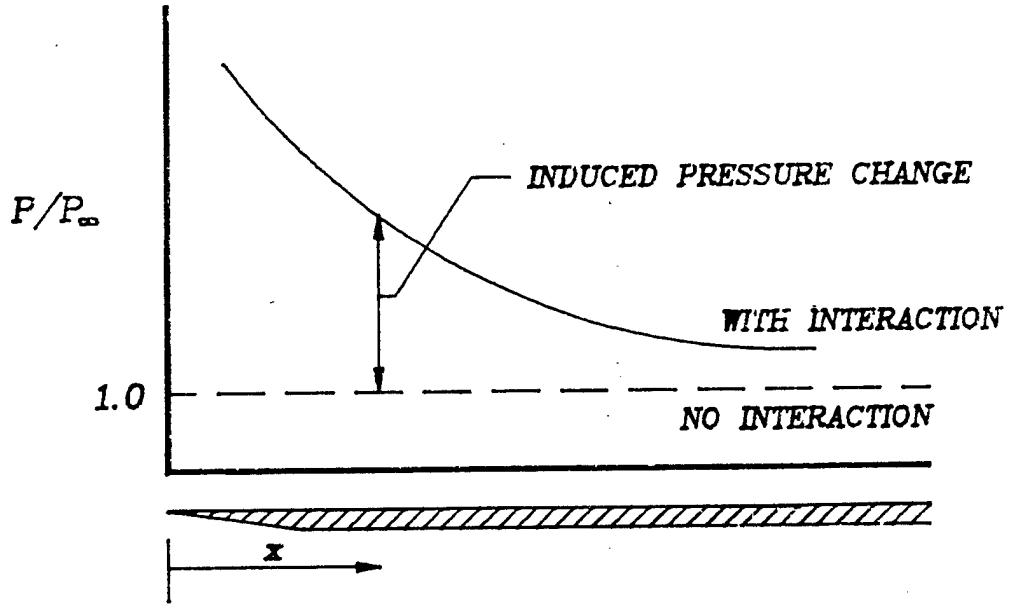

Figure 14.12 Pressure Change Due to Viscous Interaction Over a Flat Plate at Zero Angle of Attack

This increase in pressure over the no interaction case is due to a shock wave created by the boundary layer turning and compressing the streamlines. If the flat plate were at some angle of attack, the effect of the boundary layer growth would be to increase the compression angle and hence the pressure increase.

Initially, the growth of the boundary layer, $\partial\delta/\partial x$ is large and thus the effect on the pressure change is greatest. Thus the flow can be divided into a "strong interaction region" and a "weak interaction region" as shown in figure 14.13. The effect is also evident in figure 14.12.

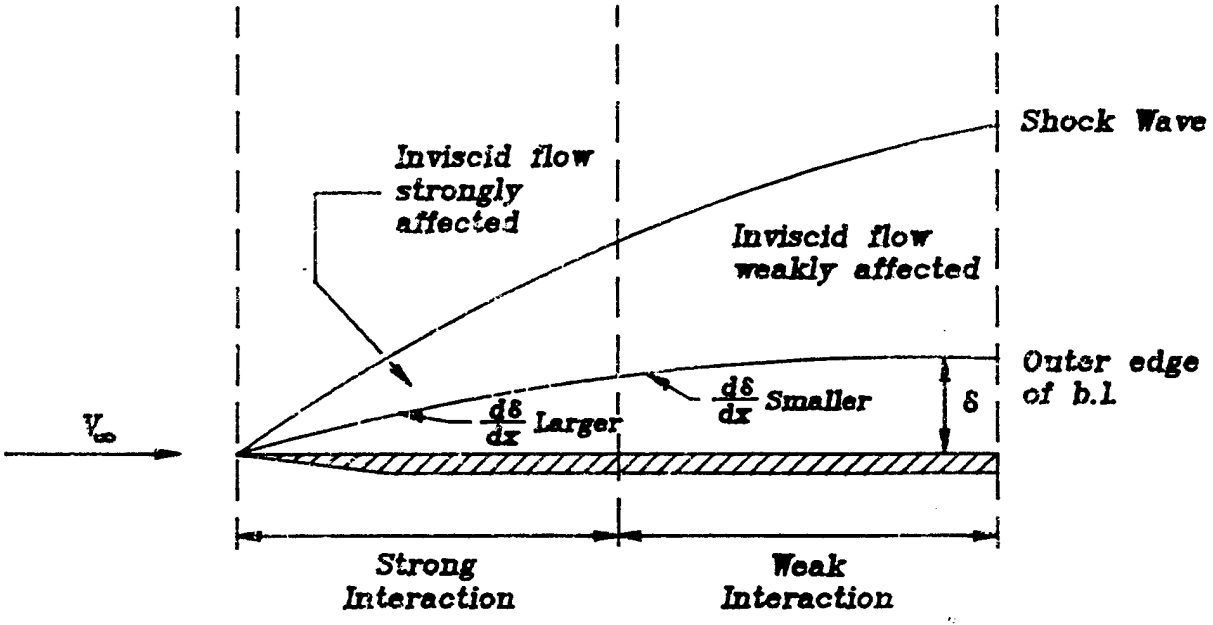

Figure 14.13 Strong and Weak Viscous Interactions

A detailed analysis of the viscous interaction phenomena proves that the parameter χ is the governing correlation parameter (ref. 3), where

$$\bar{\chi} = \frac{M_\infty^3}{R_e} \frac{\rho_w \mu_w}{\rho_\infty \mu_\infty} \qquad (14.11)$$

From reference 3, for an insulated flat plate at zero angle of attack:

Strong Interaction: $$\frac{p}{p_\infty} = 0.514\overline{X} + 0.759 \qquad (14.12)$$

Weak Interaction: $$\frac{p}{p_\infty} = 1 + 0.31\overline{X} + 0.005 \qquad (14.13)$$

Experimental verification of these results is shown in Figure 14.14. The departure from the strong interaction prediction at low values of $(AX)^{-1}$ is due to shock separation at the leading edge of the non-zero thickness "flat plate" in the wind tunnel.

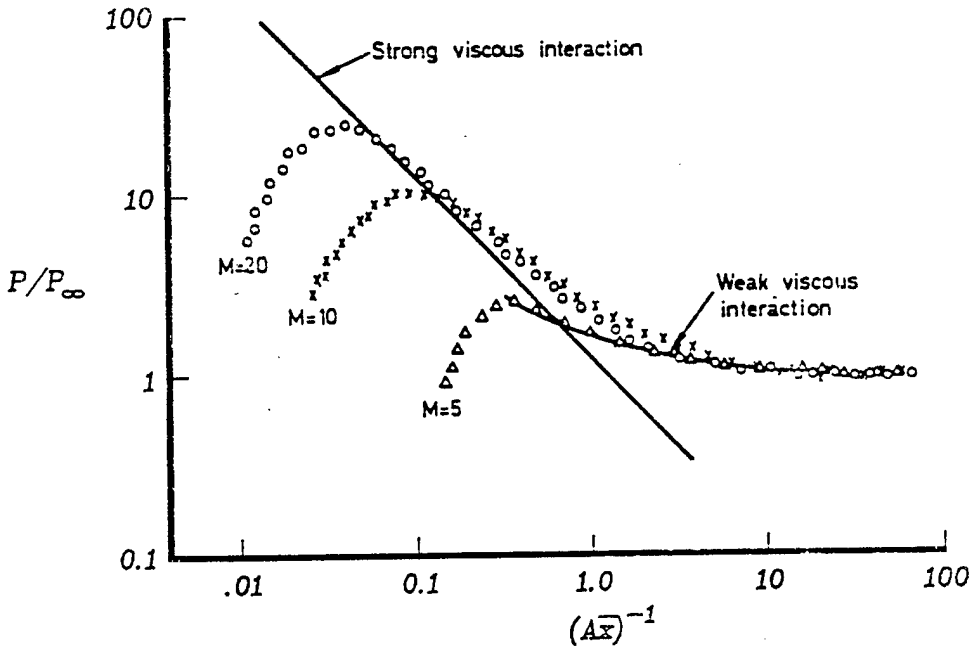

Figure 14.14 Pressure Distribution Induced on a Flat Plate at Zero Incidence

The overall effect of viscous interaction on a hypersonic flight vehicle is to increase the drag and hence reduce the lift-to-drag ratio.

14.3.3 Computational Fluid Dynamics

The viscous interactions techniques of the previous section were developed in the 1950's before the advent of modern computational capability. They are capable of providing relatively accurate predictions for a limited set of

problems based on an approximate theory. The approximation lies in separate calculations of flow characteristics in a viscous boundary layer and an outer inviscid flow, and then a coupling of these separate calculations to take into account the interaction between the two.

The aerodynamicist to calculate viscous effects exactly, simply by treating the entire flow field between the body and shock as fully viscous. No arbitrary division between a viscous boundary layer and an inviscid flow needs to be made. These methods are called computational fluid dynamics (CFD).

All CFD techniques are based on the Navier-Stokes equations. The full Navier-Stokes equations are:

Continuity equation

$$\frac{\partial \rho}{\partial t} + \nabla \cdot (\rho \mathbf{V}) = 0$$

x momentum:

$$\rho \frac{Du}{Dt} = -\frac{\partial p}{\partial x} + \frac{\partial \tau_{xx}}{\partial x} + \frac{\partial \tau_{yx}}{\partial y} + \frac{\partial \tau_{zx}}{\partial z}$$

y momentum:

$$\rho \frac{Dv}{Dt} = -\frac{\partial p}{\partial y} + \frac{\partial \tau_{xy}}{\partial x} + \frac{\partial \tau_{yy}}{\partial y} + \frac{\partial \tau_{zy}}{\partial z}$$

z momentum:

$$\rho \frac{Dw}{Dt} = -\frac{\partial p}{\partial z} + \frac{\partial \tau_{xz}}{\partial x} + \frac{\partial \tau_{yz}}{\partial y} + \frac{\partial \tau_{zz}}{\partial z}$$

Energy:

$$\rho \frac{D(e + V^2/2)}{Dt} = \rho \dot{q} + \frac{\partial}{\partial x}\left(k \frac{\partial T}{\partial x}\right) + \frac{\partial}{\partial y}\left(k \frac{\partial T}{\partial y}\right) + \frac{\partial}{\partial z}\left(k \frac{\partial T}{\partial z}\right) - \nabla \cdot p\mathbf{V}$$
$$+ \frac{\partial (u\tau_{xx})}{\partial x} + \frac{\partial (u\tau_{yx})}{\partial y} + \frac{\partial (u\tau_{zx})}{\partial z} + \frac{\partial (v\tau_{xy})}{\partial x} + \frac{\partial (v\tau_{yy})}{\partial y}$$
$$+ \frac{\partial (v\tau_{zy})}{\partial z} + \frac{\partial (w\tau_{xz})}{\partial x} + \frac{\partial (w\tau_{yz})}{\partial y} + \frac{\partial (w\tau_{zz})}{\partial z}$$

where

$$\tau_{xy} = \tau_{yx} = \mu\left(\frac{\partial v}{\partial x} + \frac{\partial u}{\partial y}\right)$$

$$\tau_{yz} = \tau_{zy} = \mu\left(\frac{\partial w}{\partial y} + \frac{\partial v}{\partial z}\right)$$

$$\tau_{zx} = \tau_{xz} = \mu\left(\frac{\partial u}{\partial z} + \frac{\partial w}{\partial x}\right)$$

$$\tau_{xx} = \lambda(\nabla \cdot \mathbf{V}) + 2\mu \frac{\partial u}{\partial x}$$

$$\tau_{yy} = \lambda(\nabla \cdot \mathbf{V}) + 2\mu \frac{\partial v}{\partial y}$$

$$\tau_{zz} = \lambda(\nabla \cdot \mathbf{V}) + 2\mu \frac{\partial w}{\partial z}$$

We used extremely simplified versions of these equations in supersonic aerodynamics. With CFD fewer and fewer assumptions need to be made.

A truly complete solution of the Navier-Stokes equations, however, is still beyond our capability. The most complete solutions to date were done at the Air Force Flight Dynamics Laboratory by J.S. Shang and S.J. Schere (ref. 6). They analyzed the entire flow field around on X-24C-10D wind tunnel model at Mach 5.95, Re = $1.64X10^7$/m, and $\alpha = 6^\circ$. The only simplifications to the Navier-Stokes equations were that they assumed steady-state conditions so that derivatives with respect to time went to zero and they used averaged Reynolds numbers. Even with these simplifications, after years of work with a large computer (a CRAY XMP-22) they were only able to get solutions for one steady state Mach number at one angle of attack. But at those conditions they got a vast amount of data which correlated very well with the wind tunnel data they had.

If you don't have the luxury of a CRAY computer and years of time to obtain data for a single flight condition, CFD is still useful if the Navier-Stokes equations are simplified a little further. One common simplification is called "parabolized Navier-Stokes" (PNS) equations. The full set of equations is simplified by assuming steady-state conditions and then dropping the viscous terms that involve derivatives in the streamwise direction. The result is a set of parabolic (hence "parabolized") partial differential equations. These are much easier to solve with a computer by starting with an initial data plane and then using a downstream marching procedure. Reference 7 gives more insight into the use and utility of PNS solutions.

Other simplifications are commonly used with CFD and it is important to know the assumptions made and limitations of a particular CFD solution. The simplest codes are capable of very quick results, the major difficulties being input of the vehicle surface matrix and extraction of data. With CFD you get every parameter imaginable (P, T, ρ, etc.) at every point in the flow. Interpreting a roomful of computer printouts is difficult and flow visualization with computer generated graphics accessing this vast data base has received a lot of attention.

14.4 HIGH TEMPERATURE EFFECTS

In supersonic aerodynamics we developed a relationship for total temperature based on static temperature and Mach, assuming a thermally perfect gas. It was:

$$T_T = T \left(1 + \frac{\gamma - 1}{2} M^2\right) \tag{14.14}$$

If this holds true at hypersonic speeds then the stagnation temperature on the space shuttle at M = 25, 100,000 ft is 51,125 °F! By way of comparison, the surface temperature of the sun is less than 11,000 °F. Therefore, we hopefully conclude that equation 14.14 does not hold at hypersonic speeds. I say hopefully, because no current materials are capable of withstanding such temperatures. Table 1 is a list of materials used in aircraft and spacecraft construction and the maximum temperature they can withstand and still be usable.

MATERIAL	TEMP (°F)
ALUMINUM	320
TITANIUM	900
INCO- 18	1300
RENE 41	1600
COLUMBIAN	2500
SHUTTLE TILE	2700

TABLE 1. MAXIMUM REUSABLE TEMPERATURE FOR SELECTED MATERIALS

The actual peak temperatures recorded on the space shuttle were under 2300 °F, thus equation 14.14 and the assumption of a thermally perfect gas obviously does not hold true at M = 25.

14.4.1 Non-Perfect Gas

The reason that equation 14.14 doesn't hold is that at higher Mach, and hence higher temperature, the perfect gas assumptions break down. The two main effects are:

a. vibration, dissociation, and ionization all absorb energy reducing T_T, and
b. The ratio of specific heats, γ, decreases with increasing temperature, approaching 1 in the limit, also reducing T_T.

For the first effect, as the gas temperature rises the force of impact between individual molecules of air becomes greater and greater. At some point during the increasing temperature, the force of individual impacts is great enough to excite internal vibration of modes of the molecules, absorbing some of the force (energy) of impact. Because of the normal distribution of velocities in a gas, some molecules will be vibrationally excited at a lower temperature, or velocity, than others. Figure 14.15 shows on an altitude velocity map where 10% and 90% of air will be vibrationally excited. As you can see, even in an SR-71 flying at Mach 3 and 80,000 ft only about 10% of the air is even vibrationally excited.

As we increase speed, the rising temperature begins to tear apart the molecular bonds, first oxygen and then nitrogen, further absorbing energy. Much later individual atoms colliding begin to knock off electrons. Air is less than 10% ionized during the normal space shuttle reentry although some ionization does occur accounting for the communications black out they experience during reentry.

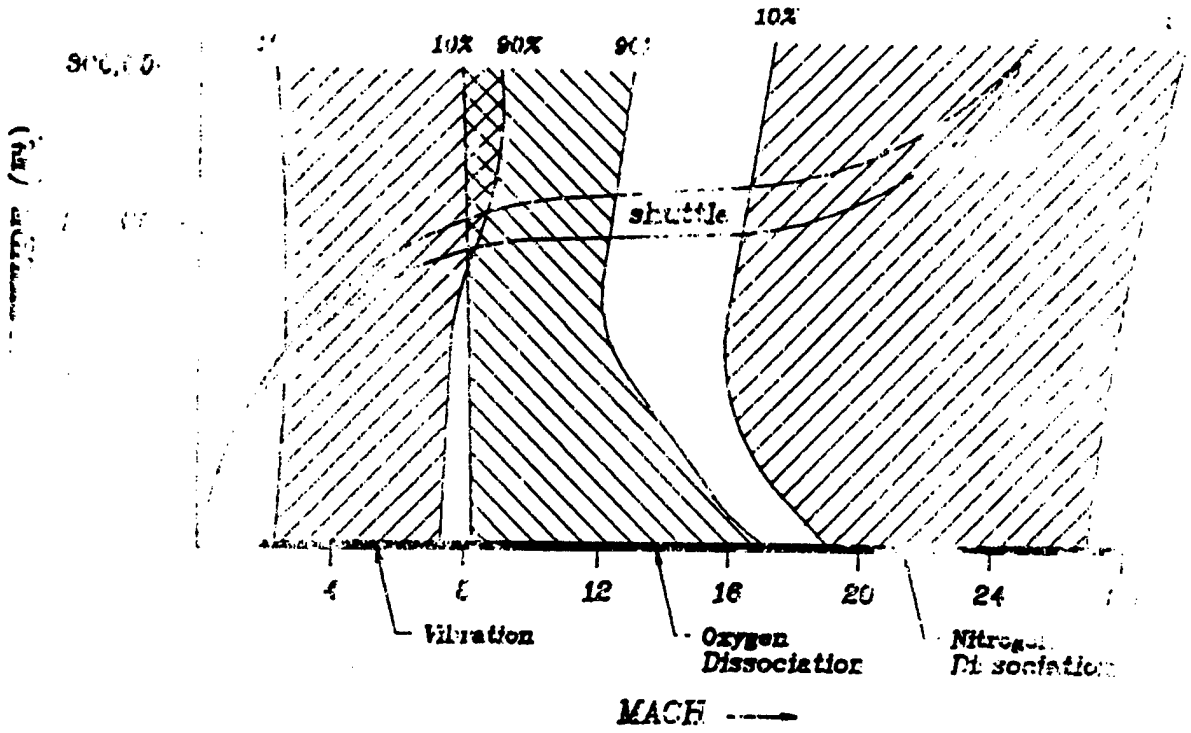

Figure 14.15 *Energy Excitation Zones for the Stagnation Point*

As the temperature increases, the number of degrees of freedom increases for the molecules in the gas. This causes γ to decrease as shown in Figure 14.16. This decrease also has a mitigating effect on T_T in equation 14.14.

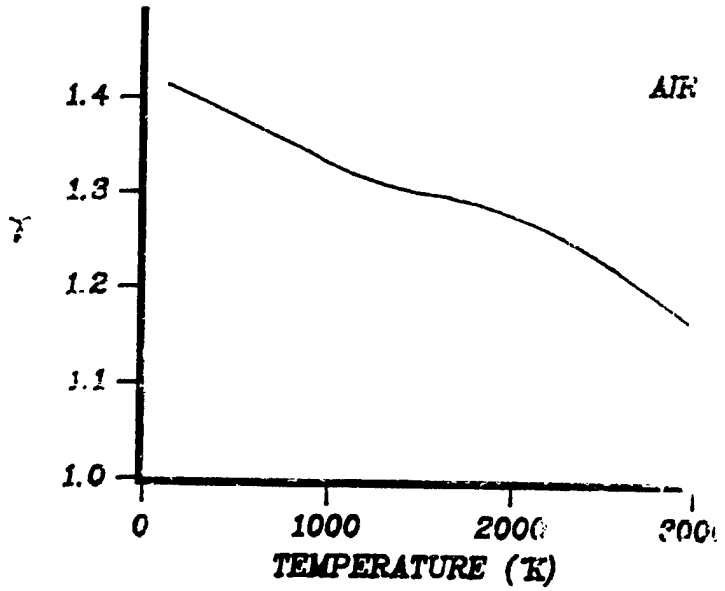

Figure 14.16. *Ratio of Specific Heats for One Atmosphere*

14.4.2 Temperature Prediction

Given the previous discussion it may appear that we could very accurately pin down the temperature on a hypersonic vehicle just by taking into account the non-perfectness of the fluid. There are, however, a few complicating factors. Four of these are briefly described here.

14.4.2.1 Radiation

Even with the mollifying effects previously described, hypersonic vehicles still become very hot. For instance, the Apollo capsule reentering the atmosphere after returning from lunar orbit ($M = 32$) had peak temperatures as high as 11,600 °K, nearly twice the surface temperature of the sun. With temperatures in the fluid this high, radiation cannot be ignored as it becomes the dominant mechanism for heat transfer. The equation for radiative heat transfer is:

$$q = K\varepsilon T^4 \qquad (14.15)$$

This doesn't seem too bad until we realize that the emissivity coefficient ε, is generally a function of temperature also. For example, there are five different types of thermal protection material on the space shuttle, all with different emissivity coefficients. Three of the five vary significantly with temperature as shown in Figure 14.17 (ref. 9). The real impact of this is on your ability to predict the temperature. A small error in T can produce a large error in ε, which in turn will affect T.

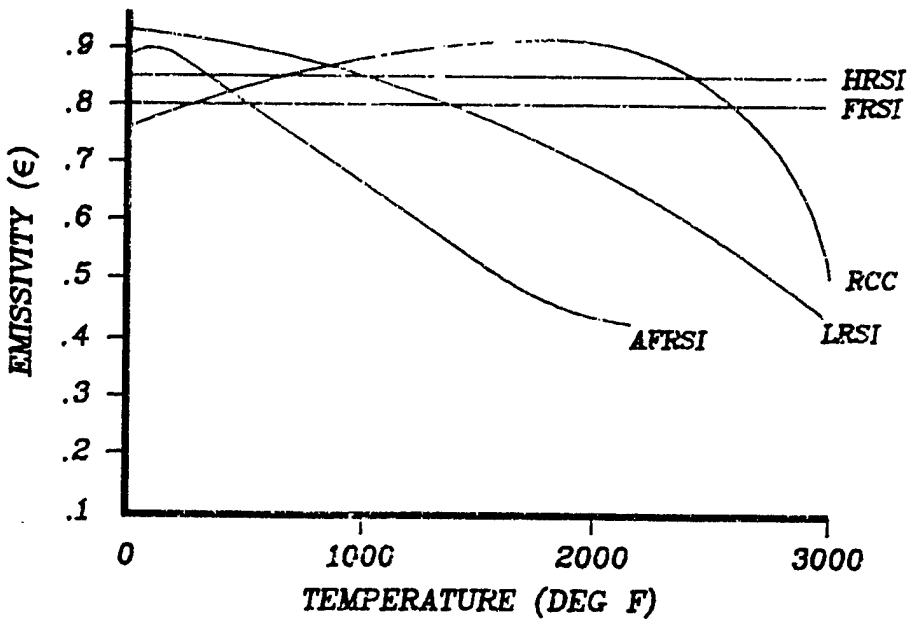

Figure 14.17 Shuttle Tile Emissivity Coefficients

14.4.2.2 Catalytic Wall Effects

Another factor complicating the prediction of temperatures is that near the surface, recombination of dissociated molecules or ionized atoms can occur at a higher rate than in the equilibrium flow. Since a large amount of energy went into the dissociation or ionization, it follows that a large amount of heat may be released by the fluid right next to the surface of our body. The extent to which a particular surface acts as a catalyst for this process is difficult to predict as can be seen in Figure 14.18. (ref. 10)

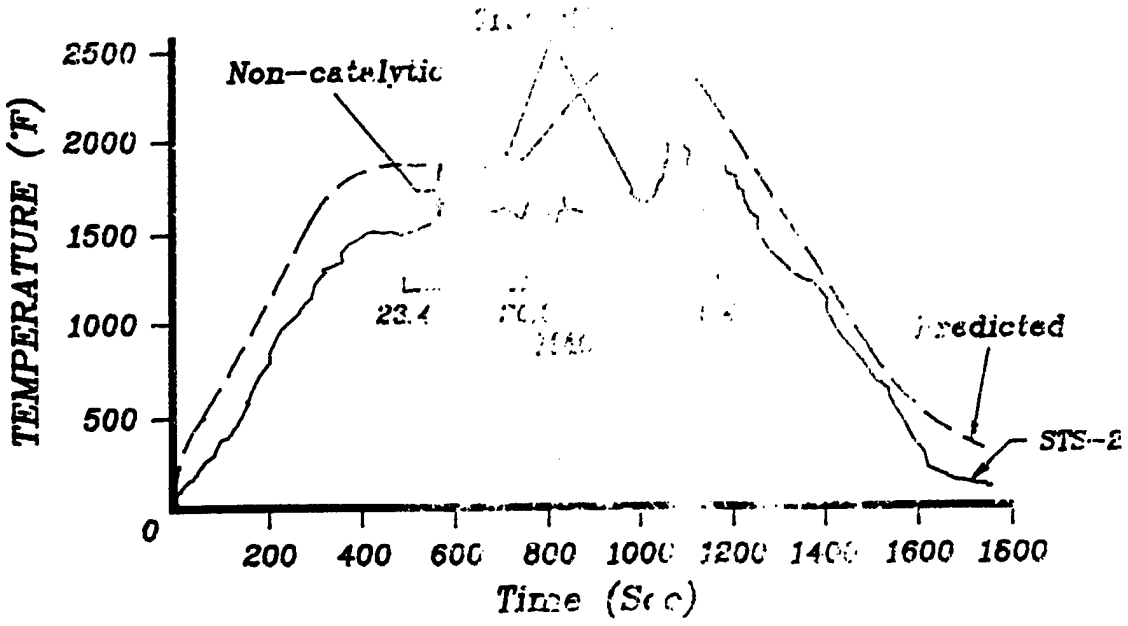

Figure 14.18 Space Shuttle Lower Surface Heating

The surface temperature prediction assumed a larger catalytic effect than was experienced causing significantly lower temperatures as can be seen on Figure 14.18 between about Mach 22 and Mach 8.

14.4.2.3 Turbulent Boundary Layer

Once the boundary layer transitions from laminar flow to turbulent the effect of conductive heating from the gas to the surface will be significantly enhanced. Predicting the point of transition is very important to predicting correct surface temperatures. Again, figure 14.18 shows that the transition is difficult to predict. The actual temperature on the lower surface made a step increase about Mach 10 indicating that this is where transition occurred instead of about Mach 15 where it was predicted.

14.4.2.4 Shock Interactions

The interactions of shock waves off of various parts of the vehicles can have very significant effects on localized heating values.

Two dramatic examples of this are the X-15 and the space shuttle. The X-15 was modified to the 'C' configuration late in the program allowing higher Mach numbers. One purpose was to test a ramjet. On the first flight of a dummy ramjet it melted off because of localized heating of the support strut due to shock impingement.

The second example is the loss of several Orbital Maneuvering System (OMS) pod tiles on the early flights of the space shuttle. Excessive heating occurred due to shock wave interactions, eventually requiring a change to a thicker tile in those areas.

14.4.3 Temperature Control

Although accurate prediction of surface temperatures of hypersonic vehicles is very difficult, the designer can control the temperatures to some extent. Two ways are by proper choice of the body shape and the choice of reentry profile.

14.4.3.1 Body Shape

Even though real air is not a perfect gas (fortunately), the vibration, dissociation, and ionization that make it non-perfect do not occur instantaneously. Thus if you quickly heat up air (say in a shock wave) then the initial temperature will be very close to that predicted assuming a perfect fluid. Later the fluid will cool, as first the collisions excite vibration modes and later as dissociation begins. Figure 14.19 shows the decrease.

In a moving fluid, the time axis in Figure 14.19 can be transposed into a distance axis. That is, as the gas flows past the shock wave, some distance is required to allow the non-perfectness of the fluid to absorb some of the temperature increase of the instantaneous shock wave. Because of this, the two bodies in Figure 14.20 will have very different surface temperatures at the leading edge.

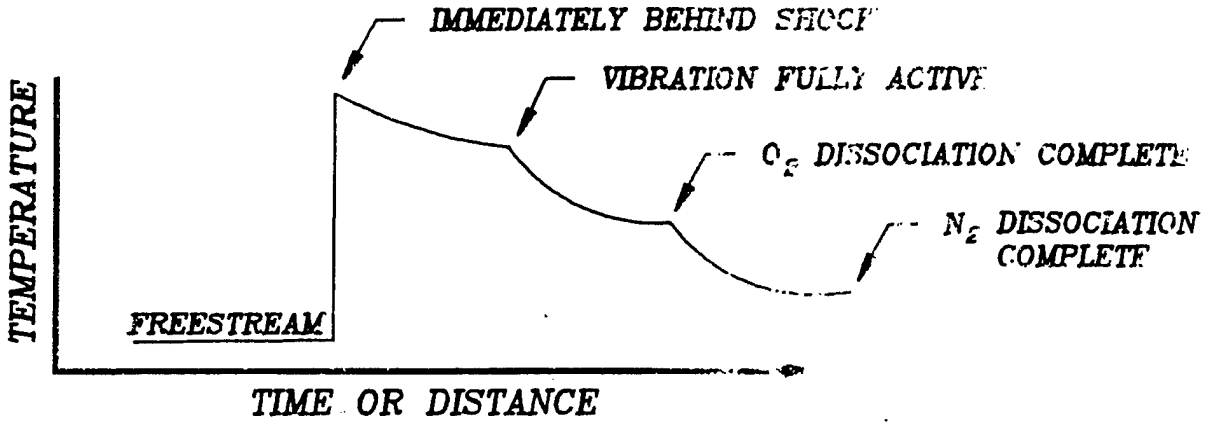

Figure 14.19 Temperature Behind a Shock Wave

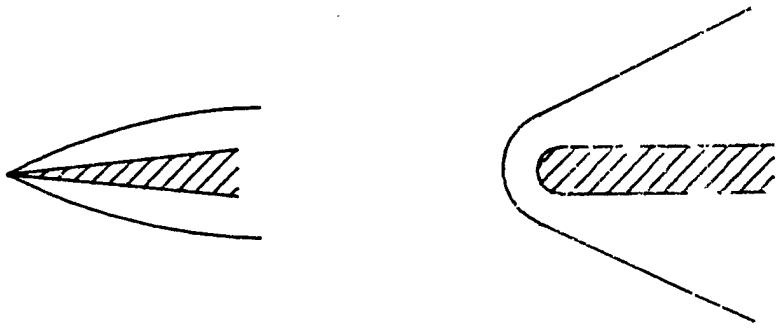

a. Sharp–nosed Attached Shock

b. Blunt–nosed Detached Shock

Figure 14.20 Sharp– vs. Blunt--nosed Slender Bodies

The sharp-nosed vehicle in Figure 14.20a will have surface temperatures at the tip approaching the perfect gas predictions. If the Mach is high enough, say orbital reentry speed, the tip would soon melt and begin to look like Figure 14.20b.

The advantage of a blunt-nosed slender body is that the detached shockwave allows the air to internally absorb some of the heat before the air reaches the surface of the vehicle.

14.4.3.2 Reentry Profile

For orbital reentry vehicles, several choices of flight path are available. Figure 14.21 shows the flight corridor bounded by lift and heat limits on an altitude-velocity map.

At very high angles of attack, range (or crossrange) is sacrificed to provide the minimum instantaneous temperature. This also allows you to expect a large temperature on only one area (e.g. the underside of the shuttle during a 40° angle of attack reentry). On the other hand, the shuttle's internal structure may reach a higher temperature due to longer exposure.
The peak temperature occurs just after landing.

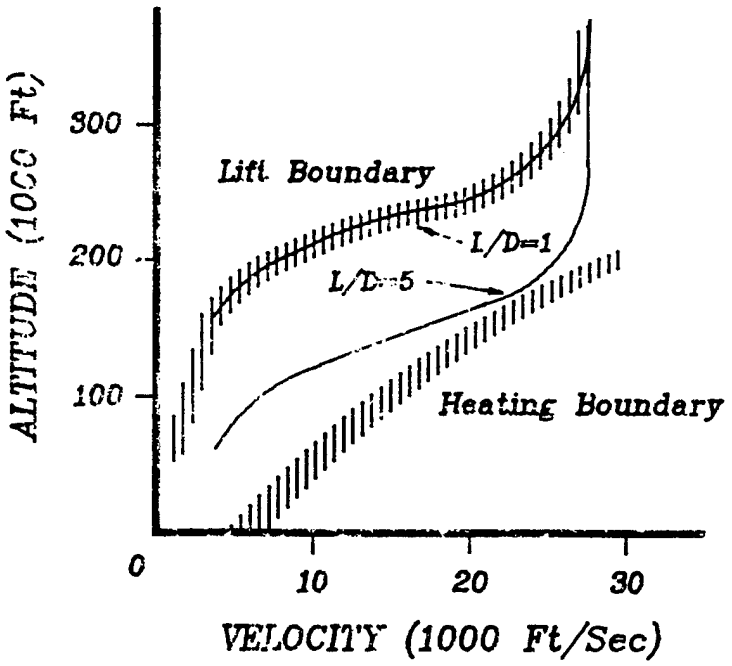

Figure 14.21 Flight Corridor

BIBLIOGRAPHY

14.1 Office of Advanced Manned Vehicles, Flight Test Results from the Entry and Landing of the Space Shuttle Orbiter for the First Twelve Orbital Flights, AFFTC-TR-85-11, Air Force Flight Test Center, Edwards AFB CA, June 1985.

14.2 Truitt, R. W., Hypersonic Aerodynamics, Ronald Press, New York, 1959.

14.3 Hayes, W. D. and Probstein, R.F., Hypersonic Flow Theory, Academic Press, New York, 1959.

14.4 NACA Report 1135. Equations, Tables, and Charts for Compressible Flow.

14.5 Anderson, John D., Jr., "A Survey of Modern Research in Hypersonic Aerodynamics", AIAA-84-1578, American Institute of Aeronautics and Astronautics, New York, 1984.

14.6 Shange, J. S., and Scherr, S. J., "Navier-Stokes Solution of the Flow Field Around A complete Aircraft", AIAA Paper No. 85-1509, 1985.

14.7 McWherter, M., Noach, R. W., and Oberhampf, W. L., "Evaluation of Boundary Layer and Parabolized Navier-Stokes Solutions for Reentry Vehicles", Journal of Spacecraft and Rockets, Vol 23, No. 1., Jan-Feb 1986.

14.8 Anderson, John D., Jr. Modern Compressible Flow with Historical Perspective, McGraw Hill, 1982.

14.9 Office of Advanced Manned Vehicles, Evaluation of the Space Shuttle Orbiter Second Orbital Flight, Descent Phase, AFFTC-TR-82-1, Air Force Flight Test Center, Edwards AFB, CA, February 1982.